Plasmon Ruler with Angstrom Length Resolution

Ryan T. Hill,[†,*] Jack J. Mock,[‡,§] Angus Hucknall,[†,⊥] Scott D. Wolter,[‡] Nan M. Jokerst,[‡,§] David R. Smith,[‡,§] and Ashutosh Chilkoti[†,⊥]

[†]Center for Biologically Inspired Materials and Material Systems, [‡]Department of Electrical and Computer Engineering, [§]Center for Metamaterials and Integrated Plasmonics, and [⊥]Department of Biomedical Engineering, Duke University, Durham, North Carolina 27708, United States

ABSTRACT

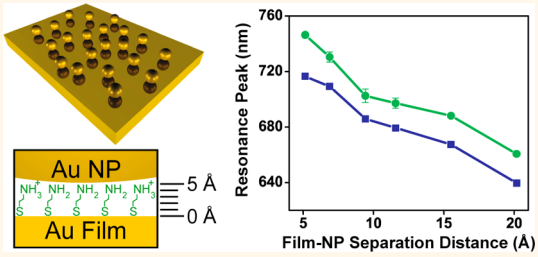

We demonstrate a plasmon nanoruler using a coupled film nanoparticle (film-NP) format that is well-suited for investigating the sensitivity extremes of plasmonic coupling. Because it is relatively straightforward to functionalize bulk surface plasmon supporting films, such as gold, we are able to precisely control plasmonic gap dimensions by creating ultrathin molecular spacer layers on the gold films, on top of which we immobilize plasmon resonant nanoparticles (NPs). Each immobilized NP becomes coupled to the underlying film and functions as a plasmon nanoruler, exhibiting a distance-dependent resonance red shift in its peak plasmon wavelength as it approaches the film. Due to the uniformity of response from the film-NPs to separation distance, we are able to use extinction and scattering measurements from ensembles of film-NPs to characterize the coupling effect over a series of very short separation distances—ranging from 5 to 20 Å—and combine these measurements with similar data from larger separation distances extending out to 27 nm. We find that the film-NP plasmon nanoruler is extremely sensitive at very short film-NP separation distances, yielding spectral shifts as large as 5 nm for every 1 Å change in separation distance. The film-NP coupling at extremely small spacings is so uniform and reliable that we are able to usefully probe gap dimensions where the classical Drude model of the conducting electrons in the metals is no longer descriptive; for gap sizes smaller than a few nanometers, either quantum or semiclassical models of the carrier response must be employed to predict the observed wavelength shifts. We find that, despite the limitations, large field enhancements and extreme sensitivity persist down to even the smallest gap sizes.

KEYWORDS: nanoparticles · gold film · localized surface plasmon resonance · plasmon coupling · plasmon ruler · sensor · nonlocal effects

We report herein characterization of the so-called "plasmon nanoruler (PNR)" in a coupled film nanoparticle (film-NP) configuration that is especially well-suited to interrogate the angstrom spatial sensitivity that should be attainable with such rulers, but that has not yet been systematically demonstrated due to experimental challenges in their fabrication. PNRs leverage the distance-dependent coupling of the surface plasmons between two or more plasmon-supporting surfaces. An early demonstration of the PNR made use of coupled plasmon resonant nanoparticle (NP) dimers, whereby DNA hybridization was visualized by a blue shift in the localized surface plasmon resonance (LSPR) of the dimer as the NPs were physically separated by DNA hybridization.[1] Since this early demonstration, the PNR effect has been further characterized, both in experimental and theoretical studies,[2−8] and has also been implemented in various biosensing schemes.[9−13] The attraction of PNRs from a sensing standpoint lies in the fact that PNRs can be extremely sensitive to distance, especially at very short separation distances, as the plasmon resonance shift as a function of distance follows a nonlinear trend that dramatically increases as the surfaces are brought closer together and generate higher field enhancements due to increased plasmonic coupling.[3−8,14,15] Furthermore, PNRs are generally sensitive over longer distances than Förster resonance energy transfer (FRET)-based rulers,[1] and signal transduction arises from an extremely bright scattering event that does not degrade over time, as is the case with photobleachable, fluorescence-based transduction.

However, the sensitivity of PNRs has been challenging to experimentally characterize because of the need to reliably exert precise control over the separation of two plasmon resonant nanostructures in three dimensions. Many of the applications of PNRs to date have involved the use of chemical linkers to create dimers of plasmon resonant NPs, which presents the following challenges. First, care must be taken to avoid colloidal flocculation during the linking process. Second, NP dimers (*i.e.*, the rulers)—as opposed to single NPs, NP trimers, or multi-NP complexes—must be

* Address correspondence to ryan.hill@duke.edu.

Received for review August 7, 2012 and accepted September 11, 2012.

Published online September 11, 2012
10.1021/nn3035809

individually selected with confidence for optical/spectroscopic analysis using spectroscopy, light polarization studies, or electron microscopy, which adds complexity to PNR analysis. These challenges have prevented access to controlled, high-throughput experimental studies within the high-sensitivity PNR regime (separation distance < ~2 nm).

Lithographic patterning of NP dimers has been instrumental in calibrating the PNR response and understanding it with theoretical analysis,[3,5,15,16] which is essential if the PNRs are to become useful metrology devices. With lithography, NP separation distance is easily set with high precision using a direct-write approach capable of creating arrays of perfectly oriented NP dimers for analysis. Hence, it is fairly straightforward to use lithography to systematically vary the NP separation distance and empirically measure the plasmonic response. These studies have helped elucidate the currently well-accepted nonlinear plasmonic coupling trend as a function of separation distance and have been used as calibration standards for many of the PR sensing studies presented to date. However, lithographically deposited plasmonic dimers are physically fixed in place, which prohibits their use as displacement sensors. Furthermore, the resolution limitations of the patterning techniques used in these studies have resulted in rather coarse step sizes, with the minimum NP separation distance being ~2 nm. While this minimum is impressive, the current understanding of plasmon coupling theory[3,5,7,14,15] suggests that significant sensitivity improvements can be realized if this separation distance can be minimized even further.

A simple approach toward creating PNRs that have the potential for increased spatial control over the plasmon-supporting surfaces is to couple plasmon resonant NPs directly to a metal film (Figure 1A), as we and others have demonstrated previously.[17−26] Here, the NP can be thought of as becoming coupled to its electromagnetic image induced within the film.[25] We create film-NP PNRs by simply functionalizing the film and/or the NPs with an organic, dielectric spacer layer of an appropriate thickness and then depositing the NPs on top of the spacer layer. The result is that every NP that is immobilized to the film becomes a PNR, and that every PNR created on the film has exactly the same alignment, which greatly simplifies their optical interrogation.[19] The use of a planar surface as the plasmonic coupling agent enables the application of a wide array of robust and tunable bulk surface functionalization and patterning techniques to create PNRs and minimizes the need to functionalize and assemble complexes of multiple NPs.

We have characterized both the PNR effect[25] and the field enhancement capabilities[19] of film-NP coupling using gold NPs separated from gold films by molecular spacer layers. In this case, the step size, or resolution, of

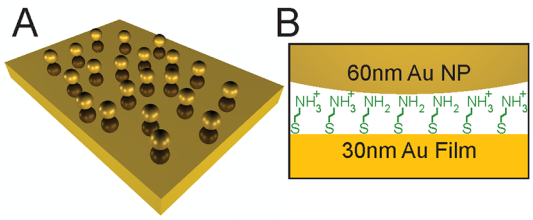

Figure 1. Film-coupled nanoparticle (film-NP) plasmon nanorulers (PNRs). (A) An ensemble of film-NP PNRs is created by coupling gold NPs directly to a gold film. NPs become coupled to their electromagnetic image induced within the film, and the film-NP plasmon resonance red shifts as the spacing between the NPs and film decreases. (B) Self-assembled monolayers (SAMs) of amine-terminated alkane thiols are used to create ultrathin gaps for film-NP PNR measurements in the angstrom regime. The cartoon in (B) is drawn to approximate scale and shows a 60 nm gold NP separated from a 30 nm gold film by an amine thiol SAM with a 2-carbon alkane chain length (*n*). A series of amine thiols with *n* of 2, 3, 6, 8, 11, and 16 were used to create film-NP spacer layers ranging from 5 to 20 Å.

the experimental PNR demonstration is limited by the thickness of the molecular spacer layers deposited on the gold films. We used layer-by-layer (LBL) deposition of polyelectrolytes (PEs)[27] to create relatively coarse PNR step sizes in these earlier studies. Through single film-NP and ensemble film-NP measurements, we have shown that the film-NP coupling effect follows the expected LSPR blue-shifting trend with increasing film-NP separation distance.[19,24,25] We note, however, that our initial characterization[25] did not show an abundantly nonlinear film-NP coupling trend with separation distance. In hindsight, we attribute this to three important factors. First, this initial study used only a handful of single film-NP scattering measurements per spacer layer to determine the average plasmonic scattering response per layer. We have shown in subsequent publications[19,24] how it is advantageous to use scattering and extinction measurements from large ensembles of film-NPs to more accurately reveal the average plasmonic response for each film-NP separation distance. Second, the initial study included a non-ideal 0 nm film-NP separation data point, which was created by incubating NPs with bare gold film and later finding NPs that had become immobilized to the film to characterize spectroscopically. As these NPs were likely physisorbed to contaminants of unknown size on the gold film, we consider these 0 nm data points to be lacking in accuracy. Third, this study, along with all of our other previous studies, did not include multiple step sizes of film-NP separation distance in the high-sensitivity PNR regime where the plasmonic coupling should be the strongest.

In this article, we build upon our previous work by experimentally characterizing the PNR in its extreme sensitivity regime (less than 2 nm film-NP separation distances) using amine-terminated alkane thiol self-assembled monolayers (SAMs, Figure 1B) with varying alkane chain lengths to create high-resolution, atomic

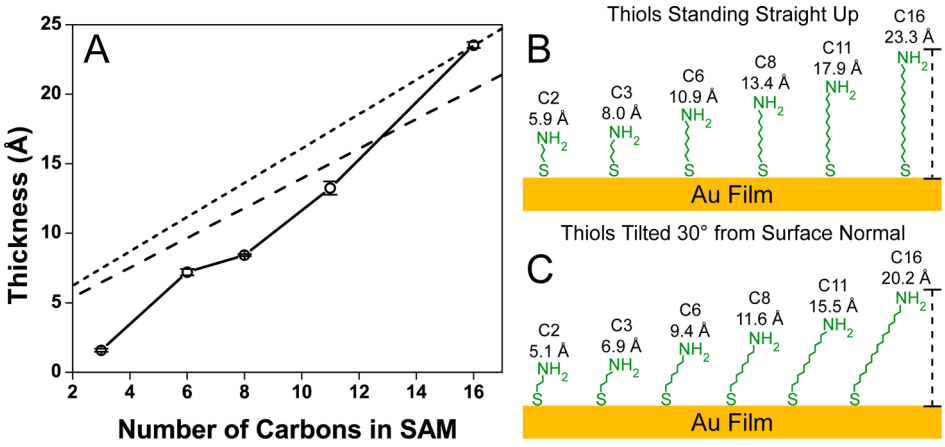

Figure 2. Amine-terminated alkane thiols with 2, 3, 6, 8, 11, and 16 carbons were used to create self-assembled monolayer (SAM) film-NP spacer layers. (A) Ellipsometric thicknesses of the layers depicted by the open circles are found to be systematically skewed relative to theoretical thicknesses of the layers with the amine thiols standing straight up on the gold film (short dashed line) as well as the case when the amine thiols are tilted by 30° relative to the normal of the gold film surface (long dashed line). Theoretical heights of amine-terminated alkane thiols are depicted standing straight up on the gold film (B) and tilted 30° relative to the gold surface normal (C).

bond length step sizes in film-NP separation distances ranging from 5 to 20 Å. Since these SAMs directly promote the chemisorption of gold NPs, we are able to make extinction and scattering measurements from ensembles of film-NPs and accurately determine the plasmonic response from each spacer layer. We combine this precise and extremely small gap dimension characterization with data from low-resolution film-NP separation step sizes extending out to ~27 nm, which allows us to probe the ultimate sensitivity limits of PNRs. Our results are supported by numerical models published elsewhere[28] that account for the nonlocal response of the conduction electrons, which begins to play a significant role when the dimensions of the nanostructures are on the order of a few nanometers or smaller.

RESULTS AND DISCUSSION

To gain access to the highly sensitive PNR regime, we created ultrathin molecular spacers on gold film by depositing SAMs of amine-terminated alkane thiols of chain lengths n = 2, 3, 6, 8, 11, and 16, where n represents the number of carbons in the alkane moiety of the molecule (Figure 1B and Figure 2B,C). These molecules were chosen for several reasons. First, amine-terminated thiols have optimal functionalities for coupled gold film/gold NP studies since the thiol end groups have a strong affinity for the gold film surfaces, which promotes self-assembly of molecularly thin monolayers.[29] Also, the terminal amine groups render the gold surface positively charged during the incubation procedure used to immobilize negatively charged citrate-stabilized gold NPs. Second, this set of molecules represents an ideal series with which to probe the ultrasensitive PNR regime because it provides six incremental separation distances within 0–2.5 nm with step sizes on the order of atomic bond lengths, as determined by the increment in n. Third, this series of molecules is conveniently available from commercial sources.

Amine thiol SAMs were formed on 30 nm thick gold films and were characterized in the dry state by variable angle spectroscopic ellipsometry. Ellipsometric thickness data from the amine thiol SAMs are plotted in Figure 2A. We were consistently unable to obtain fitted thickness values for the thinnest, C2 amine thiol layer, which we attributed to the lack of optical contrast between the extremely thin SAM and the gold film. Furthermore, extrapolation of the thickness data from the series of amine thiols produced unreasonable, negative thickness values for the C2 layers. This finding is consistent with the findings of Bain *et al.*,[30] where a similar ellipsometric characterization was performed on methyl-terminated alkane thiol and carboxy-terminated alkane thiol SAMs formed on gold films. This work demonstrated that the thicknesses of thin molecular layers as determined by ellipsometric measurements can be systematically smaller than predicted by theory. This error was attributed to the presence of ubiquitous contaminants on gold films, especially during the blank measurement of the bare gold film. This blank measurement is used to determine the unique optical constants of the bare gold film, which are used later to fit thickness values of layers subsequently added to the gold films. It can be assumed that during SAM formation at least some of the contaminants are displaced by the thiol molecules and solvent rinses, and hence, the final ellipsometric thickness measurements of the SAMs become skewed. An obvious manifestation of this measurement error is a negative y-intercept produced from linear regression of measured thickness *versus* thiol chain length data (which our data and that of Bain *et al.* produce), when the y-intercept should actually be a nonzero, positive

number representing the smallest theoretical thiol chain length.

To generate realistic thickness values for the amine thiol SAMs, we used a 3D chemical modeling program (Chem3D Pro 7.0) to calculate the theoretical lengths of each amine thiol attached to a gold atom *via* a thiolate bond using theoretical bond lengths and angles. The molecular lengths were calculated as the distance from the gold atom (representing the gold film surface) to the most distant hydrogen atom of the terminal amine group as if the molecule was standing straight up on the gold surface (Figure 2B). With the theoretical molecular lengths known, we then calculated the heights of the molecules as if they were tilted by 30° relative to the normal of the surface (Figure 2C), as it is commonly accepted that SAM formation of thiols on gold surfaces results in thiol molecules assuming some degree of tilt.[30,31] Thus, from this analysis we generated two sets of theoretical SAM spacer layer thicknesses; one set from the straight up and tilted thiol configurations, respectively. Linear regression of this molecular length *versus n* data produced a slope and *y*-intercept of 1.2 Å/carbon and 3.8 Å for the straight up thiol configuration (Figure 2A, short dashed line) and 1.1 Å/carbon and 3.3 Å for the tilted thiol configuration (Figure 2A, long dashed line). Our measured ellipsometric thickness data from three sets of amine thiol samples produced slopes and intercepts ranging from 1.6 to 2.0 Å/carbon and −6.0 to −0.9 Å when all values of *n* are included. However, when the C16 points are removed from the regression, the slopes and intercepts were 1.1−1.4 Å/carbon and −2.5−4.4 Å, which are more similar to the theoretical values. It should be expected that the slope over the range of $n = 2-16$ might not be constant in reality, as longer chain lengths of thiols tend to form more ordered and well-packed SAMs, which should result in slightly varying degrees of amine thiol tilt with varying *n*. Our ellispometric data are similar to that of Bain *et al.*,[30] where the ellipsometric thickness *versus* thiol chain length data produced somewhat reasonable slope values, compared to theoretical data, but unrealistic *y*-intercepts. We conclude from this analysis that our ellipsometric data qualitatively show SAM formation from the amine thiols, as indicated by the expected trend of increasing layer thickness with increasing *n*. However, due to limitations inherent to ellipsometry as a metrology tool in this case, the ellipsometric thickness values obtained are not accurate. Nevertheless, we find from the set of measurements and modeling that the amine thiol SAMs can provide reliable film-NP spacer layers that, according to theoretical molecular lengths, range between roughly 5 and 20 Å, in steps as small as 2 Å. This exquisite control over the spacer layer allows us to probe the most sensitive and least understood plasmonic regime.

To generate accurate PNR measurements in the extreme sensitivity regime of the film-NP ruler, we used measurements from ensembles of film-NPs in a manner comparable to that reported previously[24] to statistically average any local variations in the gold film quality, the SAM quality (which is a concern with amine-terminated thiol SAMs[32,33]), and the NP shape/size distribution. This type of measurement is only useful if the PNR fabrication process has a high yield (NP image dimer formation = 100%) and the PNR gap dimension variation is quite low. We targeted a relatively high NP surface coverage—as indicated by the optically unresolved 60 nm gold NPs and the respective scanning electron microscope (SEM) images in Figure 3—to generate easily detectable ensemble film-NP scattering and extinction. The average NP surface coverage and percentage of NP scatterer population that were composed of single NPs were calculated for each sample from SEM analysis of three 100 μm^2 areas per sample. These were found to be 2.6, 1.0, 1.5, 2.8, 2.6, and 2.4 NP scatterers per μm^2 and 97.7, 75.9, 89.5, 99.4, 99.5, and 99.9% for $n = 2$, 3, 6, 8, 11, and 16, respectively. We have shown previously that there is no significant lateral interparticle NP coupling at these levels of surface coverage.[24] We note that clean deposition of the NPs on the amine thiol surfaces required an optimized protocol relative to those used previously for deposition on PE layers (see Methods) to try to minimize the formation of NP aggregates on the SAM surfaces. Despite our efforts, however, the C3 and C6 samples still produced a significant, but low, number of NP aggregates during the NP deposition. These aggregates appeared mostly as white scatterers under dark-field microscopy, which we eliminated from our scattering data to the best of our ability *via* spatial filtering.

We characterized the plasmonic properties of the film-NP samples in the dry state (superstrate = air) using color dark-field microscope images (Figure 3A) and ensemble spectroscopic measurements (Figure 4). While we find it quite impressive that the color differences of the PNR scattering using SAM spacers of different carbon chain lengths are apparent in the Nikon D90 color images, due to the limited near-infrared sensitivity of the commercially available camera, the spectroscopic measurements are more useful for PNR characterization. Spectroscopic measurements were taken in two separate configurations. In scattering mode, we illuminate with unpolarized white light and collect the signal from the film-NP samples using a dark-field microscope objective (100×, 0.9 NA). Plots of the scattering spectra in Figure 4A show the expected blue shift in film-NP plasmon resonance scattering as the chain length of the amine thiol SAM increases. In reflectivity mode (Figure 4B), a 3 mm diameter beam of p-polarized white light was reflected off the gold film surface containing the molecular spacer layers and immobilized NPs at 70° relative to the surface normal and into a spectrometer. After normalizing to the reflectivity of the substrate containing no immobilized

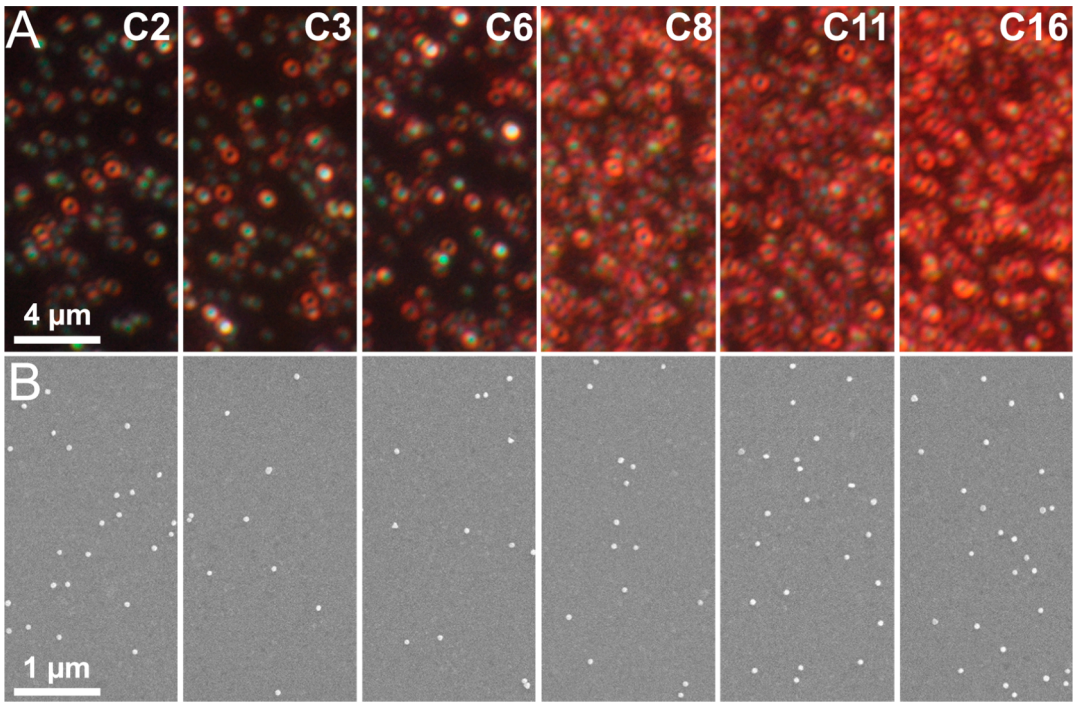

Figure 3. Images of the series of film-NP samples using amine thiol spacer layers of varying alkane carbon chain lengths (*n*, denoted by C*n*). (A) Series of dark-field microscope images (100×, 0.9 NA) showing optically unresolved 60 nm gold NPs immobilized to underlying gold film using amine thiol spacer layers of varying thicknesses. Scanning electron microscope images in (B) showing a 4×-magnified field of view relative to the dark-field images in (A) reveal the NP surface coverage on the various samples (see Results and Discussion for surface coverage statistics). High NP surface coverage was targeted for the film-NP plasmon nanoruler demonstration so as to be able to use ensemble film-NP measurements to efficiently determine the average film-NP plasmonic response to the spacer layer thickness.

NPs, we obtained spectra showing the loss of light due to the absorbance and scattering—or extinction—of incident light from the plasmon resonance of the film-NP samples. Relative to the scattering spectra in Figure 4A, the extinction spectra plotted in Figure 4B show a similar, though overall blue-shifted (Figure 4C,D), plasmon resonance shift with increasing spacer layer thickness. The consistent offset between the two lines (scattering *versus* extinction) plotted in Figure 4C,D can be attributed in the simplest terms to an increasing rate of absorption for gold at shorter wavelengths.

The differences in spectral collection configurations resulted in our spectra being produced from significantly different numbers of scatterers per measurement. The dark-field scattering measurements were made using an apertured 10 μm diameter field of view, which we used to the best of our ability to select regions of the film-NP samples that were free of NP aggregates, present mostly on the C3 and C6 samples and visible as bright white scatterers in dark-field illumination. On the basis of the NP surface coverages determined from SEM, each scattering spectrum from these film-NP samples resulted from 80 to 220 scatterers, depending on the sample. We made reflectivity measurements using a collimated 3 mm diameter beam, which probed 10s of millions of film-NP scatterers with no way of filtering out the response from any NP aggregates that were present on the samples.

Both the scattering and extinction data sets represent ensemble film-NP measurements and thus can be considered to represent a more averaged—and hence, broadened—plasmonic response from each of the film-NP samples. Nevertheless, the ensemble measurements—as opposed to accumulating single film-NP measurements one-by-one—enable efficient and accurate characterization of the thin SAMs used to probe the PNR high sensitivity regime since each spectroscopic ensemble measurement probes hundreds to millions of film-NPs at once. We demonstrate this in Figure 4C by plotting the centroid values from the scattering and extinction spectra taken from each film-NP sample *versus* the number of carbons in each SAM. These data show the ability of the PNR to outperform our ellipsometric analysis with the distinct detection of the C2 SAM, along with each of the incrementally thick amine thiol spacer layers. To gain a sense of PNR calibration with film-NP separation distance, we plot the plasmonic response of the film-NP samples against the theoretical amine thiol heights in the tilted configuration (Figure 2C) in Figure 4D. We assume here that the loosely bound citrate molecules that serve as stabilizers for the gold colloid are displaced by the amine groups,[34] which terminate our molecular spacer layers, due to amine−gold interactions.[33,35,36] We also assume that there is no deformation of the SAM spacer layers upon NP immobilization. From these data in

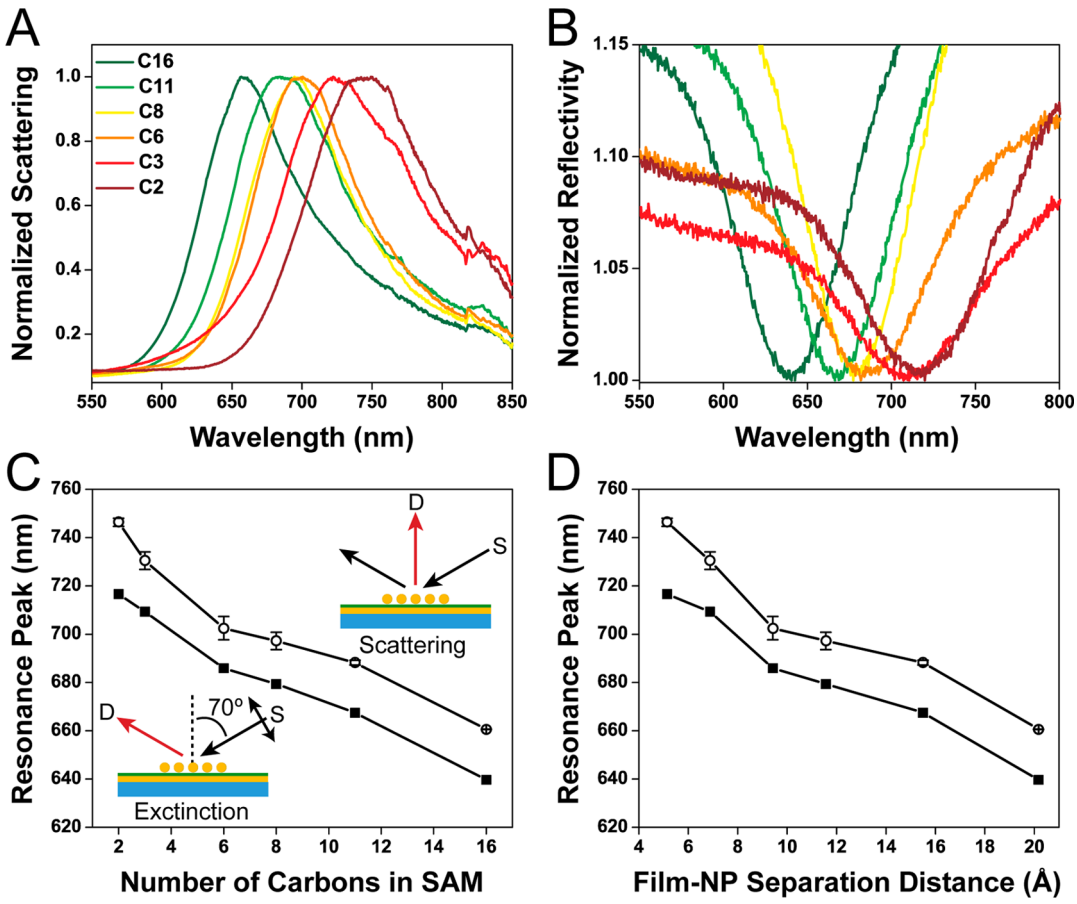

Figure 4. Spectroscopic response of the film-NP samples to variation of the amine thiol spacer layer thickness. Normalized ensemble scattering spectra (A, with instrument ray diagram in upper C inset) and extinction spectra (B, with instrument ray diagram in lower C inset) both show the expected blue-shifting plasmonic response of the film-NP samples to increasing spacer layer thickness. Peak centroids were calculated for each set of data and plotted against the number of carbons in each of the amine thiol spacer layers in (C) and against the theoretical amine thiol SAM thicknesses in (D). The scattering (open circles) and extinction (closed squares) data plotted against the film-NP spacer layer show the ability to discriminate between the number of carbon atoms in the amine thiol chain length. The same data plotted against separation distance show the ability to discern angstrom-scale changes in spacer thickness. S and D stand for source and detector, respectively.

Figure 4C,D, it is clear that the extinction follows roughly the same trend as the scattering, which suggests that the presence of a small number of NP aggregates on the C3 and C6 samples in the extinction data does not adversely affect our ability to determine the average, non-aggregated film-NP extinction values for these samples. Furthermore, the plasmonic shift per film-NP separation distance is sufficient to differentiate between the various spacer layers, some of which vary in thickness by distances on the order of single atomic bond lengths. We subjected this resonance data gathered over this small range of separation distances to a linear regression, which showed that the film-NP PNR generates a ~5 nm spectral shift in the resonance peak for every 1 Å change in film-NP separation distance when the NPs are positioned very close to the film. We note that we use a linear regression here solely for the purpose of generating a figure of merit for distance sensitivity over the PNR extreme sensitivity regime. We show in the discussion below how the data set actually follows a nonlinear trend with separation distance.

To gain further perspective on these PNR data generated from extremely thin film-NP spacer layers, we also characterized the ensemble film-NP extinction and scattering at larger spacer distances using LBL deposited PE layers[19,24,25,27] with coarse step sizes in spacer layer thicknesses extending out to ~27 nm. Figure 5A shows the resonance peak per separation distance for the combined data sets from the amine thiol SAM and PE layers. The broader view of the extinction and scattering resonance shifts with separation distance both follow a nonlinear trend, where the largest resonance shifts per distance occur when the NPs are very close (*i.e.*, < 2 nm) to the film. Both extinction and scattering data sets exhibit a high degree of linearity when plotted on a log−log scale (Figure 5B, R^2 = 0.99337 for extinction and 0.99622 for scattering), which indicates that the plasmonic film-NP coupling can be fitted quite well to a power law function, as has been suggested previously.[14,24] While at first this overall trend seems reasonable, it is found from numerical simulations that, based on the

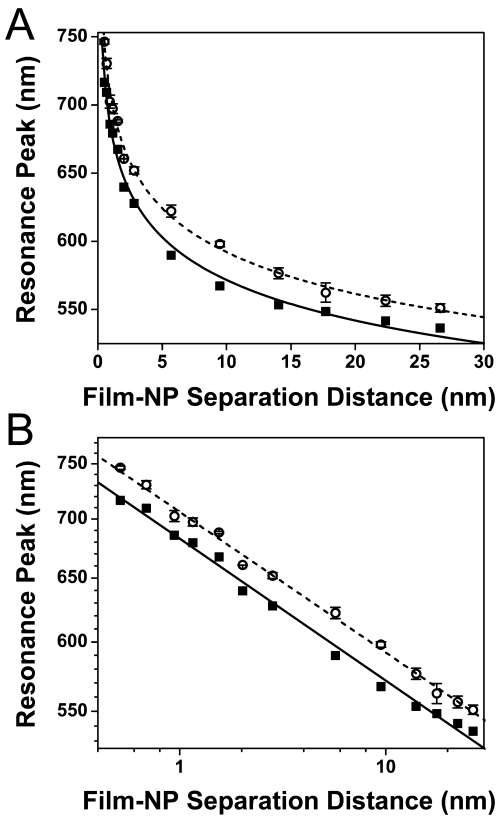

Figure 5. Spectroscopic response of the film-NP samples with spacer layers of varying thickness from 5 Å to 27 nm. Film-NP scattering (open circles) and extinction (closed squares) data shown in Figure 4D from the thin amine thiol samples are combined with data from samples using thicker polyelectrolyte spacer layers. (A) Scattering and extinction data from the film-NP samples display a nonlinear trend with increasing film-NP separation distance. (B) Same data plotted on a $\log_{10}-\log_{10}$ scale and following a linear trend, which is a signature of a power law function. Linear regression of these data produces best-fit functions of $y = -0.07652x + 2.8489$ ($R^2 = 0.99622$) for the scattering data (dashed line) and $y = -0.07719x + 2.83434$ ($R^2 = 0.99337$) for the extinction data (solid line). These functions are also displayed in (A) as the power functions $y = 706.155x^{-0.07652}$ for scattering (dashed line) and $y = 682.873x^{-0.07719}$ for extinction (solid line).

standard Drude response of the metal, there should be a substantial deviation for spacer layers smaller than ~2 nm, and thus, one should expect that the power law would not persist down to the smallest gap sizes. In recent theoretical studies, two related mechanisms have been identified that are expected to significantly alter the properties of plasmon scatterers with extreme dimensions. The first is the possibility of quantum tunneling,[37−39] in which charge transfer between the film and NP can be expected to occur. The second mechanism relates to the hydrodynamic model of the conduction electrons, which includes a quantum pressure term that accounts in an approximate manner for electron−electron repulsion.[40−42] Both models predict striking behavior for plasmonic structures with features or gaps on the subnanometer scale—the exact scale that we can access using the film-NP system presented here.[28] Our group has recently shown[28] that, upon careful inspection, the plasmon resonance spectral shifts observed for extremely small film-NP gap dimensions reveal the expected deviation from the conventional Drude model, indicating that one or more of the proposed mechanisms gains predominance. We recently developed theory and numerical simulations[28] taking into account the hydrodynamic model of electron response that has predicted spectral shifts for dimers and film-NPs consistent with our experimental measurements, suggesting that in the film-NP system studied here, nonlocality of the field-induced polarized surface charges is possibly one of the more dominant mechanisms. Taking the various theoretical approaches into account, we believe that the data shown here demonstrate what should be at, or at least very close to, the absolute distance sensitivity limit achievable for PNRs. Additionally, we believe that even though the data and theory we present suggest slight deviations at very short gap dimensions (*i.e.*, less than ~25 Å), the power law functions shown here should prove to be useful predictive design tools as they provide reasonable fits of the overall response of the film-NP PNR over a wide range of separation distances, especially at gap dimensions that will become most useful for sensing and device applications.

CONCLUSIONS

We have shown that the coupled film-NP system provides an excellent opportunity to experimentally characterize PNRs in a high sensitivity regime. The use of the coupled film-NP format is advantageous here because it greatly simplifies the task of creating uniform, intimately spaced plasmonic structures. We used a series of extremely thin bifunctional SAMs to serve as ultrashort film-NP molecular spacer layers as well as thicker PE molecular layers to probe larger separation distances. We characterized the film-NP spectral response to separation distance using measurements from ensembles of film-NPs, which enabled efficient and accurate determination of the average film-NP plasmon resonance over large populations of film-NP scatterers. We found that over the extremely short film-NP gap dimensions of 5−20 Å, the film-NP PNR outperformed our ellipsometric spacer layer characterization and produced a plasmonic resonance shift of 5 nm for every 1 Å change in film-NP distance, which, given current spectrometer resolutions, suggests that careful implementation of PNRs could result in the ability to make atomic-scale distance measurements. This distance sensitivity is 8.3 times greater than our initial film-NP PNR sensitivity report of ~6 nm spectral shift for every 1 nm change in distance[25] and ~50 times greater that of the initially reported DNA linked dimer PNRs, where ~1 nm spectral shifts per 1 nm distance changes were reported.[1] The high sensitivity reported here is due mainly—material and surrounding

medium differences aside—to the fact that these film-NP ruler measurements are made using plasmonic structures separated by extremely small distances, where the plasmonic coupling changes dramatically with subtle changes in distance. Finally, the film-NP system is a useful tool for addressing one of the most challenging regimes of plasmonics to study. Achieving reliable and reproducible subnanometer gap features enables the ultimate coupling and field enhancements to be explored; it is precisely in this regime that the greatest benefits from plasmonic media are expected. The spectral properties of film-NPs provide a measurable feature that can be used to gain information about the fundamental electron processes occurring within the metal, including quantum effects and nonlocality. In short, the film-NP system should prove to be a useful tool to explore the ultimate limits and possibilities associated with plasmonics.

METHODS

Film-NP Molecular Spacer Layer Preparation. Thirty nanometer gold films were deposited by an electron beam evaporator (CHA Industries) at 2 Å/s onto clean room cleaned Nexterion Glass B slides (Schott North America, Inc.) using a 5 nm chromium adhesion layer (deposited at 1 Å/s). Polyelectrolyte (PE) spacer layers of up to 27 nm thickness were prepared by layer-by-layer (LBL) deposition[27] of poly(allylamine)hydrochloride (PAH, M_w = 70 kDa, Aldrich) and polystyrene sulfonate (PSS, M_w = 70 kDa, Aldrich). For each deposition step, the gold-coated glass slides were immersed in 0.003 moles-of-monomer/L (monomol/L) PE and 1 M NaCl for 30 min, rinsed thoroughly with a gentle stream of ultrapure water (18 MΩ, used throughout), and immersed in fresh ultrapure water for 1 min, after which the substrates were either immersed in 1 M NaCl for 30 s before repeating the same steps for deposition of the oppositely charged PE or dried with a stream of high-purity nitrogen for analysis. All LBL depositions were initiated and terminated with the cationic PAH layer to facilitate both the attachment of the first PE layer to the gold film through amine−gold interactions[33,35,36] and the electrostatic immobilization of gold nanoparticles to the PE spacer layer.

Self-assembled monolayers (SAMs) of amine-terminated alkane thiols on gold films were fabricated using using chain lengths of n = 2, 3, 6, 8, 11, and 16 where n equals the number of carbon atoms along the alkane portion of the molecule. Amine thiols of n = 2, 3, 6, and 11 were purchased from Sigma-Aldrich (product numbers 30070, 739294, 733679, and 674397, respectively), and amine thiols of n = 8 and 16 were purchased from Dojindo (product numbers A424 and A458, respectively). All thiols were used as received. The SAMs were fabricated by incubating a gold slide in a clean glass vial containing a 1−5 mM thiol solution in 200 proof ethanol for 18 h. Following the incubation, the vials containing the gold slides and thiol solutions were sonicated in a water bath at low power (power "4" out of "10" using a Crest Ultrasonics model 230D sonicator) for 2 min and then overflow rinsed with five reaction volumes of 200 proof ethanol. This sonication and rinsing step was performed a total of four times for each slide before removing the slide from the ethanol solution and drying it with a stream of high-purity nitrogen.

We investigated several SAM formation techniques to create the most optimal amine-terminated alkane thiol SAMs for film-NP PNR studies. The goal of these studies was to create SAMs that would promote immobilization of large numbers of NPs on the SAMs without producing NP aggregates. Guided by a recent publication,[32] we made a series of amine thiol SAMs using gold slides that had been exposed to UV-ozone cleaning for 5 min (Jelight Company Inc., UVO Cleaner model no. 42, samples were ∼5 mm away from the UV source) and then incubated in acidic amine thiol solutions (5.71 mL of 1.0 N HCl added to 34.29 mL of ethanolic amine thiol solutions) in hopes of preventing the amine groups from interacting with the gold films by keeping them in a protonated form and forming more ordered SAMs. However, we had several problems with these samples. First, these samples produced erratic ellipsometric thickness data. Second, these samples produced SAMs that displayed extremely low water contact angles, which presumably indicated a highly hydrophilic surface. This should be expected with well-ordered amine-terminated SAMs. However, we believe that this extremely low contact angle inhibited our ability to deposit NPs on the film cleanly and non-aggregated. As contact angle decreases, the NP droplet applied for NP immobilization spreads further, which we hypothesize promotes more evaporation and hence more NP aggregate formation during the NP deposition step. Third, we found that film-NP samples created using this method contained unacceptable amounts of NP aggregates, and thus we could not use data generated from these samples. We also briefly investigated the use of only UV-ozone cleaning of gold before SAM formation. C2 amine thiol SAMs created using UV-ozone cleaning also created surfaces with lower water contact angles than when UV-ozone cleaning was not used. However, the film-NP extinction from the C2 SAM did not differ significantly from the case where UV-ozone cleaning was not used. For this reason, we chose not to use the UV-ozone cleaning since we are under the impression that that lower contact angles produced by this method adversely affect our ability to cleanly deposit single NPs onto the films. Thus, we found that gold films that had been subjected to no pretreatment other than storage in absolute ethanol from the time of gold film deposition to the time of SAM fabrication produced the most reproducible film-NP samples. While it may seem that lack of rigorous cleaning would produce SAMs with less overall long-range order (*i.e.*, uniformity and lack of defects over large surface areas), we found that fabricating the SAMs in this way was the best compromise for creating clean film-NP samples.

NP Deposition. Sixty nanometer gold NPs (BBI) were electrostatically immobilized on the top surfaces of each molecular spacer layer. Deposition of the gold NPs onto the PE layers was done by applying ∼400 μL drops of the undiluted stock solution of gold colloid to each PE-functionalized gold film for an incubation time of ∼30 min in a humidity chamber followed by rinsing with ultrapure water and drying with a stream of high-purity nitrogen. For the PE layers, this NP deposition procedure produces a uniform population of single film-NPs with an average surface coverage of 5.1 scatters/μm^2 and 99.6% of those scatterers being single film-NPs.[24] Deposition of gold NPs onto the amine-terminated alkane thiol SAM layers required an optimized protocol in an attempt to reduce the number of NP aggregates that formed during the deposition process. It is not yet clear as to why the NP deposition on the amine thiol layers produces more NP aggregates than deposition on the PE layers. This remains under investigation. The NP deposition procedure on the amine thiol SAMs began by placing a 200 μL drop of the undiluted stock solution of gold colloid onto a 22 × 22 mm^2 glass coverslip. Next, the downward facing functionalized gold film was lowered over the droplet until capillary action initiated by contact caused the droplet to spread out onto the film and the coverslip to be picked up by the slide. The slide remained upside down for 30 min, allowing the spherical NPs to attach to the surface of the film while discouraging aggregates from accumulating, followed by rinsing the coverslip off the surface with ultrapure water and drying under a stream of nitrogen. Scanning electron microscopy (SEM, FEI XL30 SEM-FEG) analysis of three 100 μm^2 areas per sample was used to determine the NP surface coverage of each sample (see Results and Discussion section for these values). Curious

is the fact that the C3 and C6 layers produced a significant amount of NP aggregates during the NP deposition despite our efforts to prevent NP aggregates. These aggregates appeared mostly as white scatterers under dark-field microscopy and were eliminated from our scattering data to the best of our ability *via* spatial filtering.

Ellipsometry. PE spacer layer thicknesses were measured using a J.A. Woolam Co., Inc., M-88 spectroscopic ellipsometer and WVASE32 software (version 3.460). Spectroscopic scans (277.5−763 nm) of each spacer layer were performed in three distinct regions of the functionalized gold films that did not contain immobilized NPs at 65, 70, and 75° relative to the normal of the surface of the slide. Ellipsometry data were analyzed using a two-layer model[43] composed of a bulk gold layer underneath an organic layer, which was used to represent the molecular layer. The thickness of each spacer layer was fitted using the Cauchy expression for a normal dispersion[44] provided by the WVASE32 software, where parameters "Thickness" and "A" of the model were fitted, leaving all other variables at the default values, such that the mean standard error of the fit was minimized. The nominal thickness of each spacer layer was determined to be the average of the three thickness measurements taken per spacer layer. The optical constants of each bare gold film were determined immediately prior to LBL depositions by taking spectroscopic scans of the bare gold films at 65, 70, and 75° and fitting n (n = refractive index in this case) and k to the known values of bulk gold, which were provided by the WVASE32 software, to account for any shifts in the optical constants due to the thicknesses of our gold films. These fitted optical constants for each gold slide were saved and used later when fitting for thickness of the molecular layers deposited onto the gold slides.

The amine thiol SAM spacer layers were also characterized by ellipsometry using the same procedure described above except for the fact that only "Thickness" (and not "A") was fitted in the Cauchy model. Fitting A produced unrealistic thickness and A values, which we assumed was due to the lack of contrast between the extremely thin molecular layers and the gold film. We were unable to obtain fitted thickness values for our thinnest C2 amine thiol layers using ellipsometry. Furthermore, we found that extrapolation of the ellipsometry thickness data produced unreasonably thin values for the C2 layers. This is supported by the findings of Bain *et al.*,[30] which is discussed in more detail in the Results and Discussion section of this article.

Film-NP Plasmonic Characterization. Plasmonic properties of the film-NPs were characterized by scattering spectra, reflectivity spectra, and color images. Scattering spectra and images were taken using a customized Nikon dark-field (DF) microscope with a 100× DF 0.9 NA objective. Glass slides containing the gold films with spacer layers and immobilized NPs were index-matched with oil to the top surface of a hemicylindrical lens. In dark-field mode, the samples were illuminated from above using unpolarized white light from a 75 W xenon lamp (Oriel). The microscope light path was directed to a Nikon D90 color camera to obtain color images. Scattering spectra were acquired using a 1 mm image plane pinhole aperture to reduce the field of view to ∼10 μm in diameter, containing small numbers of film-NPs, which enables the user to remove unwanted scattering from contaminants in the spectroscopy path. This field of view was directed through a spectrometer (Acton 2300SPI) and onto a detector (Photometrics CoolSnap HQ). All scattering spectra were background corrected by subtracting the spectrum from an apertured region of the substrate containing no film-NPs and normalized by dividing the spectrum from a white scattering standard (Labsphere) to correct for the wavelength response of the imaging system. The reflectance properties of the samples were measured by coupling white light from a 75 W xenon source (Oriel) through a 1 mm diameter multimode optical fiber, collimating lens, and p-polarizer and directing it to the sample surface at a 70° angle of incidence, relative to the normal to the sample surface. The beam diameter at the surface of the sample was approximately 3 mm. The reflected light was collected through a second identical lens fiber assembly and directed to the spectrometer where the spectrum was normalized by the reflectance spectrum of the bare gold film. Plasmon resonance peak positions were calculated by taking the centroid of the top (or bottom in the case of reflectivity spectra where peaks are "dips") 30% of the resonances observed in either the scattering or the reflectivity curves.

Conflict of Interest: The authors declare no competing financial interest.

Acknowledgment. This work was partially supported by NIH Grant R21EB009862 and by the NSF's Research Triangle MRSEC (DMR-1121107). D.R.S. and J.J.M. acknowledge partial support from the Air Force Office of Scientific Research (Contract No. FA9550-09-1-0562). R.T.H. also acknowledges support by Award Number F32EB009299 from the NIH NIBIB. Greg J. Nusz and Yu-Ju Tsai provided MATLAB code for finding centroids of plasmon resonance peaks.

REFERENCES AND NOTES

1. Sönnichsen, C.; Reinhard, B. M.; Liphardt, J.; Alivisatos, A. P. A Molecular Ruler Based on Plasmon Coupling of Single Gold and Silver Nanoparticles. *Nat. Biotechnol.* **2005**, *23*, 741–745.
2. Dhawan, A.; Norton, S. J.; Gerhold, M. D.; Vo-Dinh, T. Comparison of FDTD Numerical Computations and Analytical Multipole Expansion Method for Plasmonics-Active Nanosphere Dimers. *Opt. Express* **2009**, *17*, 9688–9703.
3. Gunnarsson, L.; Rindzevicius, T.; Prikulis, J.; Kasemo, B.; Käll, M.; Zou, S.; Schatz, G. C. Confined Plasmons in Nanofabricated Single Silver Particle Pairs: Experimental Observations of Strong Interparticle Interactions. *J. Phys. Chem. B* **2005**, *109*, 1079–1087.
4. Jain, P. K.; El-Sayed, M. A. Surface Plasmon Coupling and Its Universal Size Scaling in Metal Nanostructures of Complex Geometry: Elongated Particle Pairs and Nanosphere Trimers. *J. Phys. Chem. C* **2008**, *112*, 4954–4960.
5. Jain, P. K.; Huang, W.; El-Sayed, M. A. On the Universal Scaling Behavior of the Distance Decay of Plasmon Coupling in Metal Nanoparticle Pairs: A Plasmon Ruler Equation. *Nano Lett.* **2007**, *7*, 2080–2088.
6. Reinhard, B. M.; Siu, M.; Agarwal, H.; Alivisatos, A. P.; Liphardt, J. Calibration of Dynamic Molecular Rulers Based on Plasmon Coupling between Gold Nanoparticles. *Nano Lett.* **2005**, *5*, 2246–2252.
7. Romero, I.; Aizpurua, J.; Bryant, G. W.; Javier Garcia de Abajo, F. Plasmons in Nearly Touching Metallic Nanoparticles: Singular Response in the Limit of Touching Dimers. *Opt. Express* **2006**, *14*, 9988–9999.
8. Yang, L.; Wang, H.; Yan, B.; Reinhard, B. M. Calibration of Silver Plasmon Rulers in the 1−25 nm Separation Range: Experimental Indications of Distinct Plasmon Coupling Regimes. *J. Phys. Chem. C* **2010**, *114*, 4901–4908.
9. Agrawal, A.; Deo, R.; Wang, G. D.; Wang, M. D.; Nie, S. Nanometer-Scale Mapping and Single-Molecule Detection with Color-Coded Nanoparticle Probes. *Proc. Natl. Acad. Sci. U.S.A.* **2008**, *105*, 3298–3303.
10. Chen, J. I. L.; Durkee, H.; Traxler, B.; Ginger, D. S. Optical Detection of Protein in Complex Media with Plasmonic Nanoparticle Dimers. *Small* **2011**, *7*, 1993–1997.
11. Chen, J. I. L.; Chen, Y.; Ginger, D. S. Plasmonic Nanoparticle Dimers for Optical Sensing of DNA in Complex Media. *J. Am. Chem. Soc.* **2010**, *132*, 9600–9601.
12. Reinhard, B. M.; Sheikholeslami, S.; Mastroianni, A.; Alivisatos, A. P.; Liphardt, J. Use of Plasmon Coupling To Reveal the Dynamics of DNA Bending and Cleavage by Single EcoRV Restriction Enzymes. *Proc. Natl. Acad. Sci. U.S.A.* **2007**, *104*, 2667–2672.
13. Skewis, L. R.; Reinhard, B. M. Spermidine Modulated Ribonuclease Activity Probed by RNA Plasmon Rulers. *Nano Lett.* **2008**, *8*, 214–220.
14. Huang, F. M.; Wilding, D.; Speed, J. D.; Russell, A. E.; Bartlett, P. N.; Baumberg, J. J. Dressing Plasmons in Particle-in-Cavity Architectures. *Nano Lett.* **2011**, *11*, 1221–1226.

15. Wei, Q.-H.; Su, K.-H.; Durant, S.; Zhang, X. Plasmon Resonance of Finite One-Dimensional Au Nanoparticle Chains. *Nano Lett.* **2004**, *4*, 1067–1071.
16. Su, K.-H.; Wei, Q.-H.; Zhang, X.; Mock, J. J.; Smith, D. R.; Schultz, S. Interparticle Coupling Effects on Plasmon Resonances of Nanogold Particles. *Nano Lett.* **2003**, *3*, 1087–1090.
17. Driskell, J. D.; Lipert, R. J.; Porter, M. D. Labeled Gold Nanoparticles Immobilized at Smooth Metallic Substrates: Systematic Investigation of Surface Plasmon Resonance and Surface-Enhanced Raman Scattering. *J. Phys. Chem. B* **2006**, *110*, 17444–17451.
18. Gehan, H.; Fillaud, L.; Chehimi, M. M.; Aubard, J.; Hohenau, A.; Felidj, N.; Mangeney, C. Thermo-Induced Electromagnetic Coupling in Gold/Polymer Hybrid Plasmonic Structures Probed by Surface-Enhanced Raman Scattering. *ACS Nano* **2010**, *4*, 6491–6500.
19. Hill, R. T.; Mock, J. J.; Urzhumov, Y.; Sebba, D. S.; Oldenburg, S. J.; Chen, S.-Y.; Lazarides, A. A.; Chilkoti, A.; Smith, D. R. Leveraging Nanoscale Plasmonic Modes To Achieve Reproducible Enhancement of Light. *Nano Lett.* **2010**, *10*, 4150–4154.
20. Hu, M.; Ghoshal, A.; Marquez, M.; Kik, P. G. Single Particle Spectroscopy Study of Metal-Film-Induced Tuning of Silver Nanoparticle Plasmon Resonances. *J. Phys. Chem. C* **2010**, *114*, 7509–7514.
21. Ikeda, K.; Suzuki, S.; Uosaki, K. Crystal Face Dependent Chemical Effects in Surface-Enhanced Raman Scattering at Atomically Defined Gold Facets. *Nano Lett.* **2011**, *11*, 1716–1722.
22. Ikeda, K.; Sato, J.; Fujimoto, N.; Hayazawa, N.; Kawata, S.; Uosaki, K. Plasmonic Enhancement of Raman Scattering on Non-SERS-Active Platinum Substrates. *J. Phys. Chem. C* **2009**, *113*, 11816–11821.
23. Kim, N. H.; Lee, S. J.; Moskovits, M. Aptamer-Mediated Surface-Enhanced Raman Spectroscopy Intensity Amplification. *Nano Lett.* **2010**, *10*, 4181–4185.
24. Mock, J. J.; Hill, R. T.; Tsai, Y.-J.; Chilkoti, A.; Smith, D. R. Probing Dynamically Tunable Localized Surface Plasmon Resonances of Film-Coupled Nanoparticles by Evanescent Wave Excitation. *Nano Lett.* **2012**, *12*, 1757–1764.
25. Mock, J. J.; Hill, R. T.; Degiron, A.; Zauscher, S.; Chilkoti, A.; Smith, D. R. Distance-Dependent Plasmon Resonant Coupling between a Gold Nanoparticle and Gold Film. *Nano Lett.* **2008**, *8*, 2245–2252.
26. Nordlander, P.; Le, F. Plasmonic Structure and Electromagnetic Field Enhancements in the Metallic Nanoparticle-Film System. *Appl. Phys. B: Lasers Opt.* **2006**, *84*, 35–41.
27. Decher, G. Fuzzy Nanoassemblies: Toward Layered Polymeric Multicomposites. *Science* **1997**, *277*, 1232–1237.
28. Ciracì, C.; Hill, R. T.; Mock, J. J.; Urzhumov, Y.; Fernández-Domínguez, A. I.; Maier, S. A.; Pendry, J. B.; Chilkoti, A.; Smith, D. R. Probing the Ultimate Limits of Plasmonic Enhancement. *Science* **2012**, *337*, 1072–1074.
29. Love, J. C.; Estroff, L. A.; Kriebel, J. K.; Nuzzo, R. G.; Whitesides, G. M. Self-Assembled Monolayers of Thiolates on Metals as a Form of Nanotechnology. *Chem. Rev.* **2005**, *105*, 1103–1169.
30. Bain, C. D.; Troughton, E. B.; Tao, Y.-T.; Evall, J.; Whitesides, G. M.; Nuzzo, R. G. Formation of Monolayer Films by the Spontaneous Assembly of Organic Thiols from Solution onto Gold. *J. Am. Chem. Soc.* **1989**, *111*, 321–335.
31. Porter, M. D.; Bright, T. B.; Allara, D. L.; Chidsey, C. E. D. Spontaneously Organized Molecular Assemblies. 4. Structural Characterization of *n*-Alkyl Thiol Monolayers on Gold by Optical Ellipsometry, Infrared Spectroscopy, and Electrochemistry. *J. Am. Chem. Soc.* **1987**, *109*, 3559–3568.
32. Lee, S.-H.; Lin, W.-C.; Kuo, C.-H.; Karakachian, M.; Lin, Y.-C.; Yu, B.-Y.; Shyue, J.-J. Photooxidation of Amine-Terminated Self-Assembled Monolayers on Gold. *J. Phys. Chem. C* **2010**, *114*, 10512–10519.
33. Michota, A.; Kudelski, A.; Bukowska, J. Molecular Structure of Cysteamine Monolayers on Silver and Gold Substrates: Comparative Studies by Surface-Enhanced Raman Scattering. *Surf. Sci.* **2002**, *502*, 214–218.
34. Sardar, R.; Shumaker-Parry, J. S. Asymmetrically Functionalized Gold Nanoparticles Organized in One-Dimensional Chains. *Nano Lett.* **2008**, *8*, 731–736.
35. Marinakos, S. M.; Chen, S.; Chilkoti, A. Plasmonic Detection of a Model Analyte in Serum by a Gold Nanorod Sensor. *Anal. Chem.* **2007**, *79*, 5278–5283.
36. Wallwork, M. L.; Smith, D. A.; Zhang, J.; Kirkham, J.; Robinson, C. Complex Chemical Force Titration Behavior of Amine-Terminated Self-Assembled Monolayers. *Langmuir* **2001**, *17*, 1126–1131.
37. Esteban, R.; Borisov, A. G.; Nordlander, P.; Aizpurua, J. Bridging Quantum and Classical Plasmonics with a Quantum-Corrected Model. *Nat. Commun.* **2012**, *3*, 825.
38. Marinica, D. C.; Kazansky, A. K.; Nordlander, P.; Aizpurua, J.; Borisov, A. G. Quantum Plasmonics: Nonlinear Effects in the Field Enhancement of a Plasmonic Nanoparticle Dimer. *Nano Lett.* **2012**, *12*, 1333–1339.
39. Zuloaga, J.; Prodan, E.; Nordlander, P. Quantum Description of the Plasmon Resonances of a Nanoparticle Dimer. *Nano Lett.* **2009**, *9*, 887–891.
40. Fernández-Domínguez, A. I.; Wiener, A.; García-Vidal, F. J.; Maier, S. A.; Pendry, J. B. Transformation-Optics Description of Nonlocal Effects in Plasmonic Nanostructures. *Phys. Rev. Lett.* **2012**, *108*, 106802.
41. Fuchs, R.; Claro, F. Multipolar Response of Small Metallic Spheres: Nonlocal Theory. *Phys. Rev. B* **1987**, *35*, 3722–3727.
42. Toscano, G.; Raza, S.; Jauho, A.-P.; Mortensen, N. A.; Wubs, M. Modified Field Enhancement and Extinction by Plasmonic Nanowire Dimers Due to Nonlocal Response. *Opt. Express* **2012**, *20*, 4176–4188.
43. Tronin, A.; Lvov, Y.; Nicolini, C. Ellipsometry and X-ray Reflectometry Characterization of Self-Assembly Process of Polystyrenesulfonate and Polyallylamine. *Colloid Polym. Sci.* **1994**, *272*, 1317–1321.
44. Cant, N. E.; Zhang, H.-L.; Critchley, K.; Mykhalyk, T. A.; Davies, G. R.; Evans, S. D. Fabrication and Characterization of Self-Assembled Nanoparticle/Polyelectrolyte Multilayer Films. *J. Phys. Chem. B* **2003**, *107*, 13557–13562.